Coupled-Mode Theory and Its Applications in Nonlinear Optical Systems with the Analysis of Frequency-Modulated Optical Parametric Oscillation

Taran Anusorn (ta25476)

Introduction

Coupled-mode theory (CMT), a perturbational way of analyzing oscillatory systems [1], can be dated back to the early 1950s when it was first used to analyze microwave waveguides [2]. The concept of CMT is powerful for describing interaction between different modes and their dynamics in various systems. For applications in optics and photonics, CMT enables an efficient way to model energy transfer between waveguides, cavities, and surroundings as well as shifts in resonance frequencies in resonators. Apart from linear interactions, CMT can also describe the overall behavior of light and its systems under the influences of extraordinary effects, such as absorption, gain, nonlinear interactions, and Fano resonances [3], [4]. Furthermore, CMT simplifies the analysis and numerical simulation of complex systems by expressing the second-order partial differential equation (PDE) as one or more coupled first-order ordinary differential equations (ODEs).

This paper reviews the fundamental groundwork and formation of CMT, starting with the concept of modes and coupling of modes. Then, applications of temporal CMT (TCMT) [4], [5] in optical systems are revisited. A systematic approach for the utilization of TCMT in both linear and nonlinear systems is presented. Since this rather abstract idea is better understood by example, this paper specifically summarizes the analysis of comb formation in a frequency-modulated optical parametric oscillation (FM-OPO) via TCMT [6]. Finally, the conclusions highlight the implications and future directions for research in this field.

Modes and Coupling of Modes

Before delving into CMT, first introduce the concept of modes in electromagnetics, which can vary depending on different contexts. In waveguides, modes represent different discrete eigenvalues of the wave equation. These eigenvalues correspond to specific spatial field distributions, and each mode is characterized by its unique propagation constant and field pattern. For free-space waves, modes may represent different polarization states, such as linear, circular, and elliptical polarizations. In cavities, modes represent the resonant field distributions that can exist within the confined space. In general, the electromagnetic mode represents a specific distribution of electromagnetic power that *exists independently* and is *distinct from other modes*. In many situations, modes can be coupled with one another, and we can generally classify them into *spatial* and *temporal* couplings [1].

The spatial coupling occurs when modes interact through their spatial overlap or proximity. In this form of coupling, energy is exchanged between modes as they propagate through space [1]. This principle underlies the operation of waveguide couplers used in microwaves and optics. In waveguide couplers, for instance, a portion of the energy from one mode can be transferred to another mode in a nearby waveguide, as depicted in Fig. 1a [7]. Spatial coupling can also arise in periodic structures such as gratings [8] or helices in devices like backward-wave oscillators [9], where modes interact due to the periodic nature of the structure.

Temporal coupling, on the other hand, refers to an interaction between modes that occurs over time. This type of coupling typically involves nonlinear effects or external modulations, where the energy exchange between modes is not a result of proximity, but rather of dynamic interactions that evolve over time [1]. Temporal coupling is especially prominent in systems where modes share a common spatial domain, such as

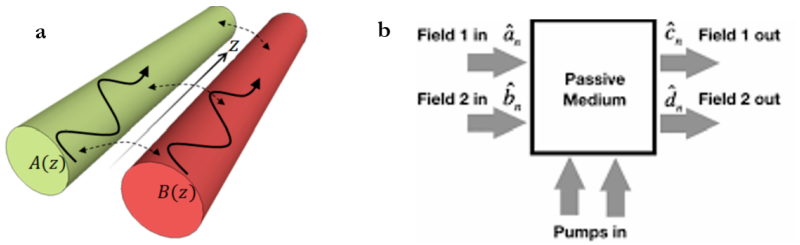

Figure 1 | Coupling of modes. a, Spatial coupling of modes between two adjacent waveguides (adapted from [7]). **b,** Temporal coupling of modes inside a nonlinear material (adapted from [10]).

in optical cavities (Fig. 1b.) or nonlinear waveguides. Given the focus of this paper on nonlinear systems, we will consider only TCMT in the subsequent discussions.

Temporal Coupled-Mode Theory

TCMT attempts to reduce the complexity of any resonant system with arbitrary material composition and geometrical configuration by simplifying such systems into a set of idealized components, such as harmonic oscillators and waveguides [4], [5]. This significantly reduces the mathematical complexity to a set of time-dependent ODEs called *coupled-mode equations* (CMEs) [5]. It is worth mentioning that the set of CMEs is universal for a certain class of device.

A. Derivation of Coupled-Mode Equations for Linear Systems

The derivation of CMEs typically starts with a wave equation that describes any system of interest and the definition of mode amplitude a_n, which normally represents a complex time-varying field amplitude of that mode. Note that the modes of the systems can be either *localized* modes, which represent energy storage inside the cavity, or *propagating* modes that correspond to waveguide modes that transport energy [5]. For example, one may consider a lumped resonator governed by [4]

$$\frac{da_n}{dx} = (i\omega_n - \gamma)a_n, \tag{1}$$

where ω_n is the resonant mode frequency and γ represents attenuation of the resonator. By including excitation of the incident wave, Eq. (1) then becomes

$$\frac{da_n}{dx} = (i\omega_n - \gamma)a_n + \mu_e s^+, \tag{2}$$

where s^+ is a complex amplitude of the incident wave and μ_e corresponds to and μ_e is a coupling coefficient. Notably, Eq. (2) undoubtedly leads to its compliment

$$s^- = cs^+ + d_e a_n, \tag{3}$$

where s^- is the amplitude of the output wave, c is scattering coefficient, and d_e outcoupling coefficient, which related to μ_e and γ.

For systems consisting of multiple cavities, the mutual couplings between different cavity mode can then be described by

$$\frac{da_n}{dx} = (i\omega_n - \gamma)a_n + \sum_{m \neq n} \mu_{c,nm} a_m, \tag{4}$$

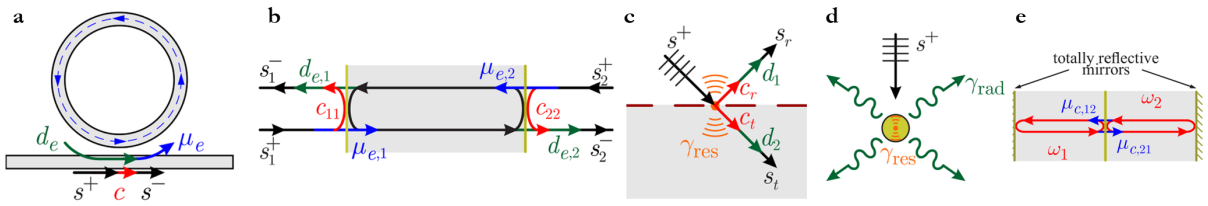

Figure 2 | Linear systems described by TCMT. a, Coupling between resonance mode in an integrated ring resonator and wave propagating in an integrated waveguide. **b,** Bidirectional propagation within the Fabry-Perot cavity causes a standing wave. Two-transparent mirrors allow for interaction with light at both ends of the cavity. **c,** A metasurface induces anomalous transmission and scattering of light through different, but coupled, processes. **d,** Isolated free-space scatterer. **e,** Direct mutual coupling between two cavities. γ_{res} corresponds to resistive loss, which can be interpreted as another port of the system (adapted from [4]).

where $\mu_{c,nm}$ represents a coupling between modes n and m. It must be mentioned that this is under the assumption that those modes are weakly coupled.

Equations (2) to (4) can effectively describe a variety of linear systems, as illustrated in Fig. 2. Note that the parameters in those equations must be rigorously determined from the physical properties of the systems. This can be done by performing full-wave simulations or directly measured from the actual systems.

B. Normalization

Normalization involves scaling variables and parameters in the CMEs to make them dimensionless and comparable in magnitude. This process simplifies the equations, improves numerical stability, and aids in identifying dominant nonlinear effects [4]. The specific choice of normalization parameters depends on the system and the dominant nonlinearity being studied. The time variable is often normalized using a characteristic time constant, such as the photon lifetime (τ) of the cavity, while mode amplitudes are normalized by either characteristic power levels, such as saturation power associated with saturable absorption, or characteristic energies.

C. Perturbation Theory

Perturbation theory states that a solution to any complex problem can be approximate by finding an exact solution to a related, simpler problem (unperturbed) and then adding small *perturbative* corrections [11]. The solution can be typically expressed as a power series in the small parameter ε:

$$A = A_0 + \sum_{n=1}^{N} \varepsilon^n A_n, \tag{5}$$

where A_0 is the solution to the unperturbed problem and subsequent terms represent increasingly smaller corrections. This method is widely applied in various fields of physics, mathematics, and engineering, particularly in quantum mechanics, celestial mechanics, and dynamical systems.

Equations. (2) and (4) are obviously first-order perturbative calculations since we assume a weak interaction between modes. The same concept of first-order perturbation theory can also be applied to systems with multiple loss channels by evaluating perturbative effects using integrals of the unperturbed eigenmode and its spatial interaction with perturbation [5]. We will see later in this paper how the first-order perturbation can be applied to obtain the CMEs, especially when we want to include nonlinearities to the calculation. Additionally, higher-order perturbation theory enhances the accuracy of analyses in more complex scenarios, such as dispersive materials and resonant states in nanophotonic structures [12], [13].

Apart from deterministic phenomena, perturbation theory can be applied to include stochastic processes, such as thermal noise [14] and spontaneous emission [15] as well.

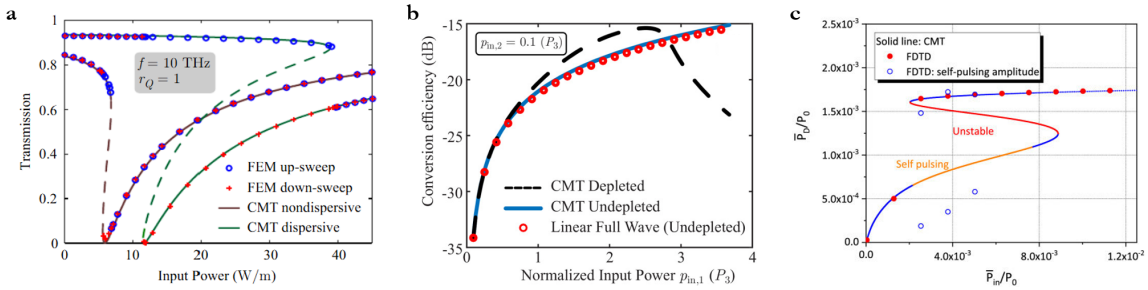

Figure 3 | Comparisons between TCMT predictions and full-wave simulations. a, Optical bistability in a graphene plasmonic traveling-wave resonator with (CMT dispersive and FEM up-sweep) or without (CMT nondispersive and FEM down-sweep) considering the dispersion of graphene, adapted from [17][16]. Incorporating the dispersion of graphene's linear electromagnetic characteristics into the TCMT framework with the correct calculation of Q-factor and self-phase modulation (SPM) parameter is vital for accurate results. **b,** Conversion efficiency of the degenerate four wave mixing (DFWM) process in a graphene plasmonic standing-wave cavity, adapted from [18]. **c,** Stationary nonlinear response of coupled optical microring resonators made of material exhibiting instantaneous Kerr nonlinearity, adapted from [19].

D. Inclusion of Nonlinearities

To include nonlinear effects, such as parametric amplification, higher-harmonic generation, and saturable absorption, in CMEs, the nonlinear contributions are treated as perturbations to the original linear system. The general process for including nonlinear effects in CMT involves presenting nonlinear effects in terms of a nonlinear polarization $\vec{P}$ and/or current density $\vec{J}$. The specific form of these quantities depends on the material and the type of nonlinearity involved. Nevertheless, it is common to account for the shift in the complex resonance frequency $\tilde{\omega}_n = \omega_n + i\gamma$ [4]:

$$\frac{\Delta\tilde{\omega}_n}{\omega_n} = \frac{\iiint \vec{P}\cdot\vec{E}_n^* dV - i\frac{1}{\omega_n}\iiint \vec{J}\cdot\vec{E}_n^* dV}{\iiint \varepsilon_0 \frac{\partial\{\omega \mathrm{Re}\{\varepsilon_r\}\}}{\partial\omega}\vec{E}_n^*\cdot\vec{E}_n dV + \iiint \mu_0 \frac{\partial\{\omega \mathrm{Re}\{\mu_r\}\}}{\partial\omega}\vec{H}_n^*\cdot\vec{H}_n dV + \iiint \frac{\partial \mathrm{Im}\{\sigma\}}{\partial\omega}\vec{E}_n^*\cdot\vec{E}_n dV}. \quad (6)$$

This expression is strictly accurate only for Hermitian systems, in which eigenvalues are all real and the corresponding eigenvectors are orthogonal. For more general cases of non-Hermitian systems, the approach of *quasinormal modes perturbation theory* is presented by introducing nonconjugated fields to the calculation [16].

The ability to account for a variety of phenomena occurring inside the systems without the need for fitting makes CMT applicable to numerous emerging nonlinear systems. Figure 3 compared the results predicted by TCMT and well-established full-wave numerical simulations, including a finite-difference time-domain (FDTD) method or a finite-element method (FEM). The comparisons highlight the accuracy and effectiveness of the TCMT, which demands much less computational power than those methods. Apart from in a graphene plasmonic traveling-wave resonator [17], a graphene plasmonic standing-wave cavity [18], and coupled optical microring resonators illustrated in Fig. 3, TCMT also demonstrates an ability to accurately model cascaded OPO processes [20] and a combination of EO modulation and OPO [6]. Furthermore, the applications of TCMT extend towards the modeling of quantum phenomena, including bipartite oscillator interactions, quantum optical memory, and mode squeezing [10]. Beyond purely optical processes, TCMT is also useful to describe systems with interactions across multiple physical domains, for instance, the analysis of electromechanical couplings in nano- and microelectromechanical systems (N/MEMS) [21].

To illustrate the usefulness of TCMT as well as the systematic way to utilize this perturbative theory to model and predict the responses of nonlinear optical systems, the remainder of this paper is dedicated to the analysis of the FM-OPO comb dynamics.

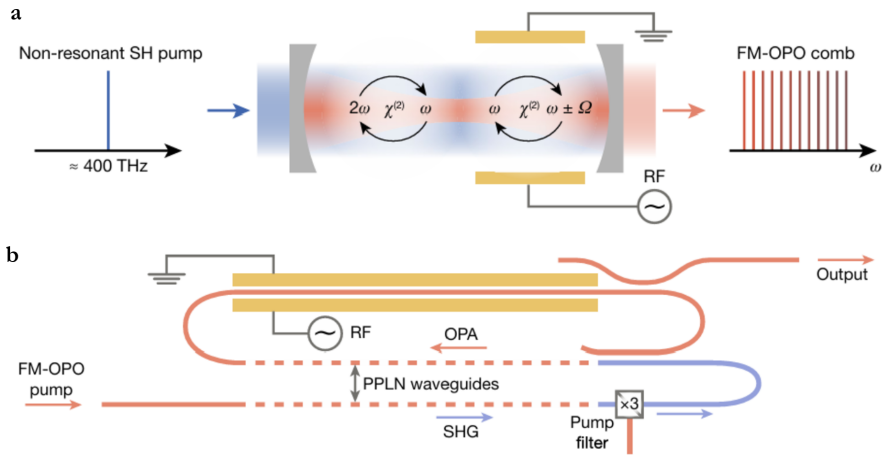

Figure 4 | The operation of FM-OPO cavity. a, The FM-OPO is the cavity that uses the SH as a pump and emits light at the FH frequency. The SH pump is converted to FH modes through second-harmonic nonlinear interaction of optical parametric amplification (OPA). The EO modulator couples adjacent FH cavity modes, resulting in an evenly distributed comb with a flat amplitude profile. **b,** The FM-OPO device has a racetrack with an intracavity coupler, where only FH modes can resonate while allowing SH to traverse the device once. The straight section of the racetrack is made of a periodically poled lithium niobate (PPLN) waveguide, designed to compensate for the effective index mismatch between FH and SH modes. The $\chi^{(2)}$ nonlinearity of the PPLN causes OPA, while on-chip electrodes couple the FH modes to RF signals. The input PPLN waveguide on the chip converts the FH pump from a commercially available C-band laser to the SH pump of the cavity via another nonlinear interaction called second-harmonic generation (SHG). Three on-chip intracavity coupler filters prevent the FH pump from entering the cavity as well as define the cavity boundary. Adapted from [6].

Analysis of Frequency-Modulated Optical Parametric Oscillation Using Temporal Coupled-Mode Theory

A. Physical Dynamics of Frequency-Modulated Optical Parametric Oscillation

Unlike existing microcomb technologies relying on electro-optic (EO) or Kerr effects, the FM-OPO utilizes a combination of electro-optic modulation and parametric amplification within a thin-film lithium niobate (TFLN) cavity [6]. The operation of the FM-OPO comb, as illustrated in Fig. 4, starts with the feed of an optical pump that closes to the resonance frequency of the cavity. A strong $\chi^{(2)}$ nonlinearity of the TFLN waveguide generates second harmonic (SH) signals, doubling the frequency of the original pump. The efficient SH generation is achieved through the compensation of effective index mismatch between FH and SH modes using a periodically poled waveguide. Intracavity filters then suppress the fundamental harmonic (FH) pump, meaning that there is only the SH pump that enters the cavity. It must be noted that the researchers designed the cavity to operate as a doubly resonant cavity, in which the SH passes through the cavity in a non-resonant manner, and only FH modes oscillate inside this cavity.

Within the cavity, an optical parametric amplification through the $\chi^{(2)}$ nonlinearity results in FH modes with mode frequencies ω_n specified by the cavity's free spectral range (FSR, denoted by ζ_1) and second-order dispersion ζ_2 [6]:

$$\omega_n = \omega_0 + \zeta_1 n + (\zeta_2/2)n^2, \tag{7}$$

where ω_0 is the resonance frequency of the cavity. Note that n can be either negative or positive integer. By introducing EO modulation with a drive frequency near to the FSR, the coupling between FH modes occurs simultaneously with the optical parametric oscillation (OPO). The processes avoid a transition to mode-locking, which means there is no pulse formation. Instead, the comb formation behaves like the operation of

frequency-modulated (FM) lasers, obtaining a continuous frequency-sweeping output. In terms of performance, the SH pump efficiently converts to the FH comb with 93% depletion inside the cavity at the optimal modulation coupling rate determined by the drive input power of RF modulator.

B. Coupled-Mode Equations of Frequency-Modulated Optical Parametric Oscillation

H. S. Stokowski *et al.* has presented the detailed derivation of the CMEs describing FM-OPO in their supplementary material of Ref. [6]. To model the doubly resonant OPO, the Hamiltonian of the system can be separated into unperturbed and interaction (OPA) parts, denoted by H_0 and H_{PA}, respectively.

$$H_0 = \sum_n (\omega_n - \frac{\omega_p}{2}) a_n^* a_n \tag{8}$$

and

$$H_{PA} = g \sum_n b a_n^* a_{-n}^* + \text{c. c.}, \tag{9}$$

where ω_p is the SH pump frequency, g is the $\chi^{(2)}$ nonlinear coupling rate, and a_n and b correspond to the amplitudes of the n^{th} FH mode around the OPO degeneracy (point $n = 0$) and the SH pump mode, respectively.

By introducing the RF modulation, the Hamiltonian must include

$$H_{mod} = 2M\cos(\Omega t) \sum_{\sigma=s,i} \sum_{m,m'} a_{\sigma,m'}^* a_{\sigma,m} + \text{c. c.}, \tag{10}$$

where M is the EO modulation rate, Ω is the RF frequency of the phase modulator, s and i represents signal and idler tones, and the indices m are the offsets from the oscillating modes:

$$a_{s,m} = a_{(n_{osc}+m)} \tag{11}$$

and

$$a_{i,m} = a_{-(n_{osc}+m)}. \tag{12}$$

The resulting classical Hamiltonian, including both the parametric gain and the modulation, is

$$H = H_0 + H_{PA} + H_{mod}. \tag{13}$$

The CMEs following this Hamiltonian are then

$$\dot{a}_n = \left[i\left(\Delta + n\delta - \frac{n^2 \zeta_2}{2} \right) - \frac{\kappa_{a,n}}{2} \right] a_n - iM(a_{n-1} + a_{n+1}) - i2g a_{-n}^* b \tag{14}$$

and

$$\dot{b} = -\frac{\kappa_b}{2} b - ig \sum_n a_n a_{-n} + i\sqrt{\kappa_b}\beta_{in}, \tag{15}$$

where $\Delta = \omega_p/2 - \omega_0$ is laser pump detuning, $\delta = \Omega - \zeta_1$ is RF-FSR detuning, $\kappa_{a,n}$ captures the loss rate of each FH mode, κ_b is the effective loss rate of the SH pump, and β_{in} represents the pump power of the doubly-resonant cavity

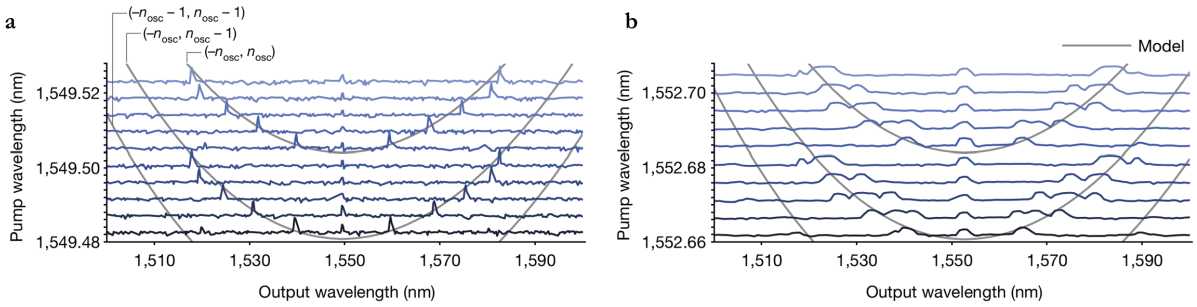

Figure 5 | Doubly resonant cavity tuning by pump wavelength. a, The blue traces are the measured output spectra of the cavity corresponding to different pump wavelengths. It is found that the frequency matching between the signal and idler modes determines the output wavelength of the cavity output. The measurements align well with the theoretical model (grey lines), which predicts the oscillations to recur every half free spectral range. **b,** The FM-OPO exhibits a similar tuning pattern (adapted from [6]).

$$P_{in} = \hbar\omega_p|\beta_{in}|^2. \tag{16}$$

Equations (14) and (15) indicate how interactions between modes influence their temporal rates of change through OPA and EO processes. Note that only the pair of n and $-n$ is considered in the OPA interaction here since the study, as illustrated in Fig. 5, shows that it has the strongest coupling at a certain operating condition. As reported in the supplementary material of Ref. [6], the authors assume that the SH mode is in a steady state, i.e., $\dot{b} = 0$, Eq. (15) reduces to

$$b = -2i\frac{g\sum_n a_n a_{-n} - i\sqrt{\kappa_b}\beta_{in}}{\kappa_b}, \tag{17}$$

C. Retrieval of Physical Parameters

Up to this point, where the CMEs of the system under study have been systematically established, additional studies are needed to determine all the required physical parameters, which are summarized in Table 1. Following Ref. [6], four key studies remain to be conducted: (1) full-wave simulation of PPLN waveguides to determine the group velocity and second-harmonic (SH) mode characteristics, (2) multiple-laser spectroscopy of the cavity at the fundamental harmonic (FH) to characterize the behaviors of FH modes, such as cavity coupling efficiency, losses, and dispersion related to OPO effects, (3) characterization of RF modulation, and (4) characterization of the fully-operated FM-OPO system.

Notably, some parameters in Eq. (14) and (17) require further clarification and interpretation of the reported values. For example, loss rate $\kappa_{a,n}$ need to be calculated from the Q-factors and the escape coefficiency of the cavity to account for all loss mechanisms of the FH associated with the FH modes. Moreover, EO induced mode-coupling rate M_0 indicates the rate of change of EO coupling rate M with the

Table 1 | Summary of the FM-OPO device parameters reported in Ref. [6]

Parameter	Units	Description	Value
Average Q_a	-	Average FH quality factor, measured by laser spectroscopy of cavity at FH.	1.0×10^6
Average $Q_a^{(i)}$	-	Average FH quality factor, measured by laser spectroscopy of cavity at FH.	1.6×10^6
$\kappa_b/2\pi$	GHz	Effective loss rate of the SH pump, calculated from simulated group velocity	3.566
η_a	-	Cavity escape efficiency, extracted from average $Q_a^{(e)}$ and Q_a	0.36
$\zeta_1/2\pi$	GHz	Cavity FSR, measured by laser spectroscopy of cavity at FH	5.7853
$\zeta_2/2\pi$	kHz	Cavity second-order dispersion, measured by laser spectroscopy of cavity at FH	−11.1
g	kHz	Nonlinear interaction rate, extracted from fitting output power of the OPO	12
$M_0/2\pi$	MHz/V	Electro-optically induced mode-coupling rate, fitted from modulated cavity transmission	60

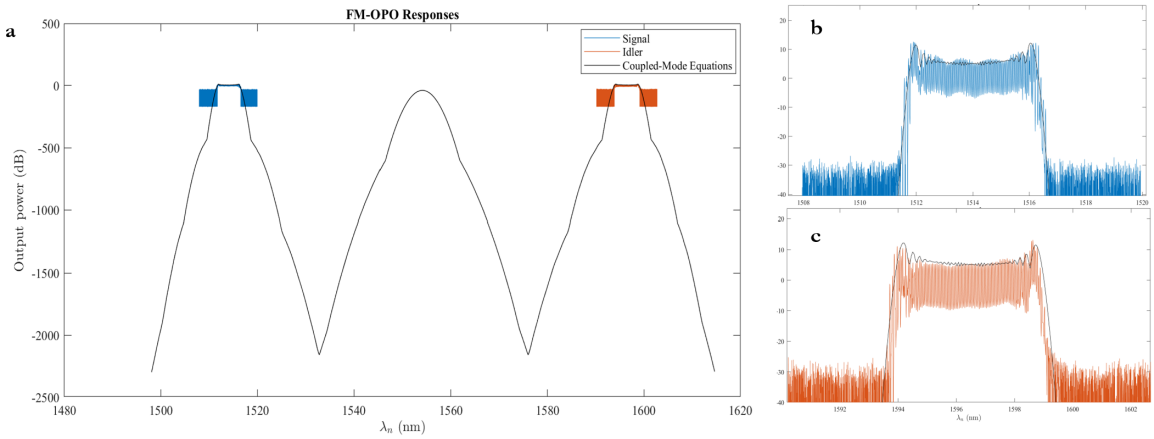

Figure 8 | FM-OPO comb output responses. a, The predicted FM-OPO response (a solid black line) is plotted alongside the measured results for the signal and idler wavelengths. The zoomed-in views of the signal and idler wavelengths are shown in panels **b** and **c**, respectively, indicating a strong agreement between theorical simulation and measurements. The plots here are plotted from the raw data provided by Ref. [6].

peak RF modulation voltage. Furthermore, a_n itself reflects the amplitude of mode *inside* the cavity. To obtain the resulting comb profile, one needs to consider the outcoupling efficiency.

D. Results and Discussions

By simultaneously solving Eqs. (14) and (17) for a large number of FH modes, namely $n = 2{,}500$ in the original paper, the FM-OPO comb profile can be determined. It is crucial to note that the comb profile is the output spectrum of the device. Moreover, a_n must be initially seeded with a nonzero value; otherwise, no dynamics would occur at all. In reality, OPOs are normally seeded by quantum vacuum. For this reason, the initial set of a_n can be set to be field amplitudes corresponding to the energy equivalent of one photon. Figure 8a. shows the responses of the FM-OPO comb, including measurement spectra around the signal and idler wavelengths and the prediction by numerical calculations of CMEs. Zoomed-in figures (Fig. 8b. and Fig. 8c) demonstrate a strong correlation between the equations and the observed formation dynamics of the FM-OPO, especially within non-degenerate regions. However, the simulation cannot capture the comb spacing, which is reported to equal the FSR of the cavity. Moreover, the dynamics of the comb in the degenerate region, i.e., around ω_0, remain for future study. To more accurately model the comb characteristics, more complex treatment and interpretation of interactions within the cavity are required. Furthermore, higher-order perturbations should be considered to assess whether they improve the accuracy of the results. In addition, it is interesting to explore how accurately the time-domain nature of the derived CMEs can model these dynamics.

Summary and Conclusion

This paper reviewed the fundamentals of coupled-mode theory (CMT), starting with the concept of electromagnetic modes and their coupling mechanisms, before narrowing the focus to temporal CMT (TCMT). It examined how TCMT simplifies the analysis of resonant systems by representing them as sets of reduced-order components. The paper also briefly addressed the formation of coupled-mode equations (CMEs) in both linear and nonlinear systems, along with a discussion of perturbation theory. Practical examples, including the analysis of the FM-OPO, illustrated the applicability and effectiveness of TCMT in modeling vibrational systems.

The main challenge of this framework lies in comprehensively accounting for all significant interactions within complex systems. Future research may focus on identifying the framework's limitations and exploring the full capabilities of this framework, such as its ability to capture the real-time dynamics of the systems.

Because CMT is perturbative, small corrections can be added to account for weak interactions or deviations. This makes it a flexible framework for improving models and dealing with systems that are getting more complicated. By systematically combining such intuitive strategies with state-of-the-art computational methods, it is possible to develop a universal tool for accurately predicting and designing advanced materials, systems, or technologies tailored to diverse applications.

References

[1] H. A. Haus and W. Huang, "Coupled-mode theory," *Proceedings of the IEEE*, vol. 79, no. 10, pp. 1505-1518, Oct. 1991, doi:10.1109/5.104225.

[2] S. E. Miller, "Coupled wave theory and waveguide applications," *Bell System Technical Journal*, vol. 33, no. 3, pp. 661–719, May 1954. doi:10.1002/j.1538-7305.1954.tb02359.x.

[3] M. F. Limonov, M. V. Rybin, A. N. Poddubny, and Y. S. Kivshar, "Fano resonances in Photonics," Nature Photonics, vol. 11, no. 9, pp. 543–554, Sep. 2017. doi:10.1038/nphoton.2017.142.

[4] T. Christopoulos, O. Tsilipakos, and E. E. Kriezis, "Temporal coupled-mode theory in nonlinear resonant photonics: From basic principles to contemporary systems with 2D materials, dispersion, loss, and gain," *Journal of Applied Physics*, vol. 136, no. 1, Jul. 2024. doi:10.1063/5.0190631.

[5] J. D. Joannopoulos, S. G. Johnson, J. N. Winn, and R. D. Meade, *Photonic Crystals Molding the Flow of Light - Second Edition*. Princeton University Press, 2011.

[6] H. S. Stokowski *et al.*, "Integrated frequency-modulated optical parametric oscillator," *Nature*, vol. 627, no. 8002, pp. 95–100, Mar. 2024. doi:10.1038/s41586-024-07071-2.

[7] T. Mealy and F. Capolino. "Exceptional points of degeneracy with indirect bandgap induced by mixing forward and backward propagating waves," *Physical Review A*, vol. 107, no. 1, Jan. 2023, doi:10.1103/physreva.107.012214.

[8] L. Cheng, S. Mao, Z. Li, Y. Han, and H. Fu, "Grating couplers on silicon photonics: design principles, emerging trends and practical issues," *Micromachines*, vol. 11, no. 7, p. 666, Jul. 2020, doi:10.3390/mi11070666.

[9] H. C. Jung *et al.*, "Transmission of gigawatt-level microwave using a beam-rotating mode converter in a relativistic backward wave oscillator," *Applied Physics Letters*, vol. 96, no. 13, Mar. 2010, doi:10.1063/1.3368692.

[10] M. G. Raymer and I. A. Walmsley, "Temporal modes in quantum optics: then and now," *Physica Scripta*, vol. 95, no. 6, p. 064002, Mar. 2020, doi:10.1088/1402-4896/ab6153.

[11] M. H. Holmes, *Introduction to perturbation methods*. New York: Springer-Verlag, 1995.

[12] H. S. Sehmi, W. Langbein, and E. A. Muljarov, "Applying the resonant-state expansion to realistic materials with frequency dispersion," *Physical review. B./Physical review. B*, vol. 101, no. 4, Jan. 2020, doi:10.1103/physrevb.101.045304.

[13] S. Both and T. Weiss, "Resonant states and their role in nanophotonics," *Semiconductor Science and Technology*, vol. 37, no. 1, p. 013002, Dec. 2021, doi:10.1088/1361-6641/ac3290.

[14] Bertrand Braeckeveldt and B. Maes, "Thermal radiation in asymmetrically driven coupled non-linear photonic cavities," *Physical review. B./Physical review. B*, vol. 107, no. 17, May 2023, doi:10.1103/physrevb.107.174310.

[15] P. Hamel *et al.*, "Spontaneous mirror-symmetry breaking in coupled photonic-crystal nanolasers," *Nature Photonics*, vol. 9, no. 5, pp. 311–315, Apr. 2015, doi:10.1038/nphoton.2015.65.

[16] T. Christopoulos, O. Tsilipakos, and E. E. Kriezis, "Perturbation theory for Kerr nonlinear leaky cavities," *Optics Letters*, vol. 45, no. 23, p. 6442, Nov. 2020, doi:10.1364/ol.408336.

[17] T. Christopoulos, O. Tsilipakos, N. Grivas, and E. E. Kriezis, "Coupled-mode-theory framework for nonlinear resonators comprising graphene," *Physical Review E*, vol. 94, no. 6, Dec. 2016, doi:10.1103/physreve.94.062219.

[18] T. Christopoulos, O. Tsilipakos, G. Sinatkas, and E. E. Kriezis, "Degenerate four-wave mixing in nonlinear resonators comprising two-dimensional materials: A coupled-mode theory approach," *Physical Review B*, vol. 98, no. 23, Dec. 2018, doi:10.1103/physrevb.98.235421.

[19] Nessim Jebali, Loïc Bodiou, J. Charrier, A. Armaroli, and Yannick Dumeige, "Combining FDTD and coupled-mode theory for self-pulsing modeling in coupled nonlinear microring resonators," *Journal of the Optical Society of America B*, vol. 37, no. 9, pp. 2557–2557, Jul. 2020, doi:10.1364/josab.399879.

[20] T. P. McKenna *et al.*, "Ultra-low-power second-order nonlinear optics on a chip," *Nature communications*, vol. 13, no. 1, Aug. 2022, doi:10.1038/s41467-022-31134-5.

[21] M. Guo *et al.*, "Mode Coupling in Electromechanical Systems: Recent Advances and Applications," *Advanced Electronic Materials*, vol. 9, no. 7, May 2023, doi:10.1002/aelm.202201305.